01 Jan 2023

Demonstration Of High Detoxification Efficiency Of Glassy Polymer-Metal Hydroxide Composites Toward Chemical Warfare Agent Simulants

Peter O. Aina

Sukanta K. Mondal

Joshua Costain

Ali A. Rownaghi
Missouri University of Science and Technology, rownaghia@mst.edu

et. al. For a complete list of authors, see https://scholarsmine.mst.edu/che_bioeng_facwork/1679

Recommended Citation

P. O. Aina et al., "Demonstration Of High Detoxification Efficiency Of Glassy Polymer-Metal Hydroxide Composites Toward Chemical Warfare Agent Simulants," *ACS Applied Polymer Materials*, American Chemical Society, Jan 2023.
The definitive version is available at https://doi.org/10.1021/acsapm.3c00918

ACS APPLIED POLYMER MATERIALS

pubs.acs.org/acsapm Article

Demonstration of High Detoxification Efficiency of Glassy Polymer−Metal Hydroxide Composites toward Chemical Warfare Agent Simulants

Peter O. Aina, Sukanta K. Mondal, Joshua Costain, Ali A. Rownaghi,* and Fateme Rezaei*

Cite This: https://doi.org/10.1021/acsapm.3c00918 Read Online

ACCESS | Metrics & More | Article Recommendations | Supporting Information

ABSTRACT: The design and development of polymeric composites that can effectively capture and destruct toxic chemicals with a fast detoxification rate is of high importance for protecting the military, first responders, and civilians. Here we report the synthesis and assessment of zirconium hydroxide ($Zr(OH)_4$)-incorporated Ultem, Matrimid, and PIM-1 composites for detoxification of dimethyl 4-nitrophenylphosphonate (DMNP), as a type G toxic nerve agent simulant. Maintaining homogeneity, three different loadings (8, 20, 30 wt %) of $Zr(OH)_4$ were incorporated into the polymers, and the thin films of composite materials were developed for subsequent hydrolysis tests. Our results indicated that increasing the $Zr(OH)_4$ loading enhances the hydrolysis rate and the amount of DMNP converted for all three polymers. While the surface area and porosity of PIM-1 reduced upon increasing $Zr(OH)_4$ loading, 30%-$Zr(OH)_4$@PIM-1 was found to be the best performing material to achieve ∼100% conversion in 2 h with a hydrolysis rate of 5.5×10^{-3} μmol/s at room temperature. It was also observed that the performance of 30%-$Zr(OH)_4$@PIM-1 is drastically improved at 60 °C by exhibiting a conversion rate of 4.9 μmol/s, while achieving 100% conversion almost instantaneously (within 5 s). Our findings represent a substantial improvement of this class of materials over previously reported polymer-metalhydroxide composites toward the detoxification of toxic gases.

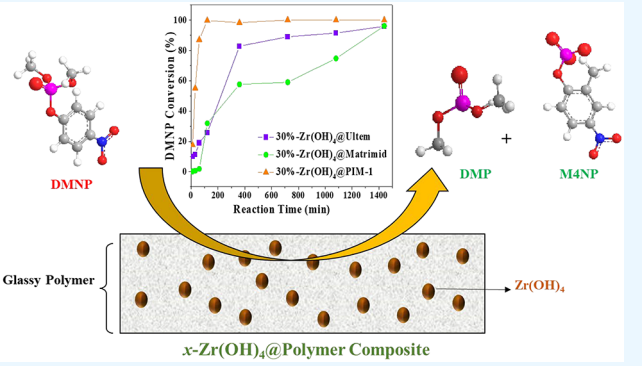

KEYWORDS: *detoxification, chemical warfare agent, hydrolysis, composites, polymer*

1. INTRODUCTION

Nerve agents such as *O*-pinacolyl methylphosphonofluoridate (GD) and *S*-(2-diisopropylamino)ethyl *O*-ethyl methylphosphonothionate (VX) are a class of chemical warfare agents (CWAs), which are known for their interference with the central nerve system by forming covalent bonds with acetylcholinesterase, resulting in accumulation of the neurotransmitter acetylcholine and thereby leading to continuous neuron stimulation.[1,2] In many countries, there have been regulations about the exposure limit of these chemicals to the public to limit its fatal effect. The United States has regulated the maximum contaminant limit to 1 ng/m^3 because research studies have shown that 50 μm/m^3 can be immediately fatal.[3−6]

Significant efforts have been put forth to design techniques by which these highly toxic agents can be destroyed effectively in a short time frame.[7,8] Due to the reactivity of numerous organophosphorus compounds with nucleophiles, researchers have extensively investigated nucleophilic substitution as a potential method for hydrolyzing organophosphorus CWAs.[9−11] However, the hydrolysis of organophosphorus compounds is a slow process, which might take up to 72 h to achieve 100% conversion to harmless products. In recent years hydrolysis reaction has been fast-tracked through coordination of the phosphoryl oxygen atom to a Lewis acid atom which eventually exposes the nerve agent to nucleophilic attack.[7,11,12]

In the bid to develop an efficient catalyst responsible for coordination of the phosphoryl oxygen atoms, various transition-metal-based catalysts (e.g., Ti, Zr, Ce, Zn) have been investigated to facilitate the fast hydrolysis of CWAs. For example, Giannakoudakis et al.[13] explored the use of bismuth titanate nanoparticles (BTO-NPs) for adsorption and degradation of mustard gas. The authors reported a 67% destruction of mustard vapor after exposure to visible light. Similarly, TiO_2-grafted graphene was studied for the destruction of 2-

Received: May 3, 2023
Accepted: July 18, 2023

chloroethyl ethyl sulfide (CEES), and the study showed maximum destruction of CEES (ca. 94.6%) after 5 days.[14]

Owing to the high surface area and microporosity, the utilization of porous polymers (such as PIMS) in detoxification of harmful gases such as nerve agents has recently evolved. In particular, reactive porous polymers are known for launching a nucleophilic attack on these nerve agents for the purpose of degrading them.[15] As such, many scientists have adopted the method of using a polymer with nucleophilic properties to accelerate the rate of hydrolysis. For example, Farha and his team investigated the effect of nucleophiles on dimethyl 4-nitrophenyl phosphate (DMNP) hydrolysis over amidoxime-functionalized PIM-1 (PIM-AX) and reported an 84% degradation of DMNP after 48 h of exposure.[16] In another study,[17] polyacrylamidoxime (PANOx) and poly(*N*-hydroxyacrylamide) (PHA) were used for degradation of GB and VX, and a half-life of 3 min was observed for the degradation of GB, while VX showed a half-life of 4.3 h. The enhanced performance was attributed to the presence of nucleophilic moieties (amide and amidoxime) in these polymers.

Limited studies in the literature have shown that metal hydroxides such as zirconium(IV) hydroxide ($Zr(OH)_4$) can enhance the hydrolysis kinetics of the nerve agents, mainly due to (i) the electrostatic interactions and bond formations between organophosphates and metal hydroxides, (ii) additional active sites provided by the $Zr(OH)_4$ to the composite materials, and (iii) complex surface chemistry and hydrolysis capability of $Zr(OH)_4$.[18−21] For instance, Bandosz et al.[19] reported a near instantaneous decontamination of VX over $Zr(OH)_4$ and linked the unprecedented performance of this detoxifying medium to its predominant surface Lewis acidic sites.

Motivated by the great advantages offered by glassy polymers, we embarked on a study to explore the enhancement of their CWAs destruction performance through the addition of $Zr(OH)_4$. Our hypothesis was that incorporation of metal hydroxide particles into the polymer matrix with optimum content can enhance the hydrolysis reaction kinetics and as a result maximize the conversion rate of the DMNP simulant to nontoxic products.[22] $Zr(OH)_4$ was selected as our metal hydroxide due to its defective cluster nature that can induce porosity in polymer network and thereby enhance the hydrolysis reaction rate.[12,19,23,24] To verify this hypothesis, three sets of glassy polymers ranging from nonporous (Ultem, Matrimid) to porous (PIM-1) materials were utilized for the degradation of DMNP. Ultem and Matrimid possess very interesting properties that make them suitable for various separation and reaction applications, including tunable permeability, amorphous thermoplastic behavior, high glass transition temperature, cost-effectiveness, self-healing, high mechanical strength, and flexibility.[25−28] On the basis of these intrinsic properties, we aimed at investigating the performance of Ultem and Matrimid for the destruction of DMNP along with PIM-1. Ultem is a poly(ether imide) polymer known for making glasses and eye goggles due to its glassy nature, but has not been investigated for the hydrolysis of CWAs so far; thus, we aimed at exploring the resonance behavior of this class of material when coupled with $Zr(OH)_4$ for the destruction of the DMNP simulant. Matrimid is a conjugated polyimide that shows a possible resonance rearrangement to initiate a nucleophilic reaction when doped with a metal hydroxide. Like Ultem, the efficacy of this material for detoxification of CWAs has not been explored in the past. $Zr(OH)_4$@polymer composites with three different loadings of $Zr(OH)_4$ (e.g., 8, 20, 30 wt %) were developed, and their physiochemical properties were thoroughly investigated. The specified percentage of the fillers was determined using a ternary phase diagram to achieve optimum composition for Zr-$(OH)_4$@polymer. The DMNP hydrolysis performance of the developed composites was then assessed via ^{31}P NMR tests to determine their efficacy in the detoxification of CWAs and their simulants.

2. EXPERIMENTAL SECTION

2.1. Materials. Poly(ether imide), commonly known as Ultem, Matrimid, 5,5′,6,6′-tetrahydroxy-3,3,3′3′-tetramethyl-1,1′-spirobisindane (TTSBI), tetrafluoroterephthalonitrile (TFTPN), dimethyl-4-nitrophenyl phosphate (DMNP), anhydrous *N*,*N*′-dimethylformamide (DMF), zirconium hydroxide ($Zr(OH)_4$), sodium carbonate (Na_2CO_3), chloroform ($CHCl_3$), tetrahydrofuran (THF), methanol, *N*-methyl-2-pyrolidone (NMP), 2-amino-2-methyl-1,3-propanediol (AMPD), *N*-ethylmorpholine (NEM), and polyvinylpyrrolidone (PVP) were purchased from Sigma-Aldrich and used in this study.

2.1.1. Preparation of Ultem and Its x- Zr(OH)$_4$@Ultem Composites. The Ultem polymer was prepared using the phase inversion method. 1.0 g of the Ultem powder was added to 6 mL of chloroform, and the polymeric solution was stirred for 24 h at 500 rpm and 50 °C.[25] After complete dissolution, the Ultem dope solution was degassed for 2 h to prevent void formation on the polymer surface. Afterward, the dope solution was cast onto a flat glass plate and covered with a glass plate. The resultant composite was later detached from the plate and dried at 85 °C in an oven for 24 h to lose the trapped solvent. Formation of *x*-$Zr(OH)_4$@Ultem composites required three different loadings of $Zr(OH)_4$ in the Ultem polymer to be prepared through homogeneous mixing and then rolling on a low-profile roller for 24 h. The resultant mixture was cast on a glass plate and dried at 85 °C in an oven. The letter *x* here indicates specified percentage of $Zr(OH)_4$ (ca. 8, 20, 30 wt %) incorporated into the Ultem polymer solution to facilitate its catalytic performance toward DMNP hydrolysis.

2.1.2. Preparation of Matrimid and x-Zr(OH)$_4$@Matrimid Composites. The solvent used for this polymer was prepared by dissolving 2.33 g of PVP in 76 mL of NMP. PVP is a pore-forming agent that was added here to induce pore formation in the Matrimid composites. The mixture was sonicated for 30 min to obtain a clear solution, followed by the addition of 5 mL of deionized (DI) water as a cosolvent to achieve uniformity. The Matrimid dope solution was prepared by dissolving 8.34 g of Matrimid in the above mixture and stirring at room temperature for 3 h. Afterward, the solution was degassed for 2 h to remove air bubbles and then cast by using a casting knife onto a glass Petri dish and kept in a vacuum chamber under ambient temperature and relative humidity of 65% overnight. The polymer was washed three times in a hot water bath to remove the residual solvent. Lastly, the washed polymer was dried at 40−50 °C in a vacuum oven for 5 h.[29] To prepare the $Zr(OH)_4$@Matrimid composites, 8, 20, and 30 wt % of $Zr(OH)_4$ were added to the Matrimid dope solution and mixed together with the aid of a magnetic stirrer to form a homogeneous paste. The paste was then transferred to the low-profile roller to achieve a uniform distribution of $Zr(OH)_4$ particles within the polymer matrix. The solution was later cast, washed, and dried in a similar manner to the bare Matrimid.

2.1.3. Preparation of PIM-1 and x-Zr(OH)$_4$@PIM-1 Composites. PIM-1 was synthesized and purified using a modified procedure described elsewhere.[30] Briefly, a three-necked 500 mL flask equipped with a mechanical stirrer was purged with N_2 for 30 min. Purified TTSBI (10.2 g, 30 mmol), TFTPN (6.0 g, 30 mmol), and anhydrous DMF (150 mL) were placed in the flask and stirred at 140 rpm until the monomers were dissolved. Next, K_2CO_3 (8.3 g, 60 mmol) and DMF (50 mL) were added to the solution. The flask was immediately immersed in a preheated oil bath at 55 °C and stirred for 72 h. The reaction solution was precipitated upon cooling by slowly pouring it

https://doi.org/10.1021/acsapm.3c00918
ACS Appl. Polym. Mater. XXXX, XXX, XXX−XXX

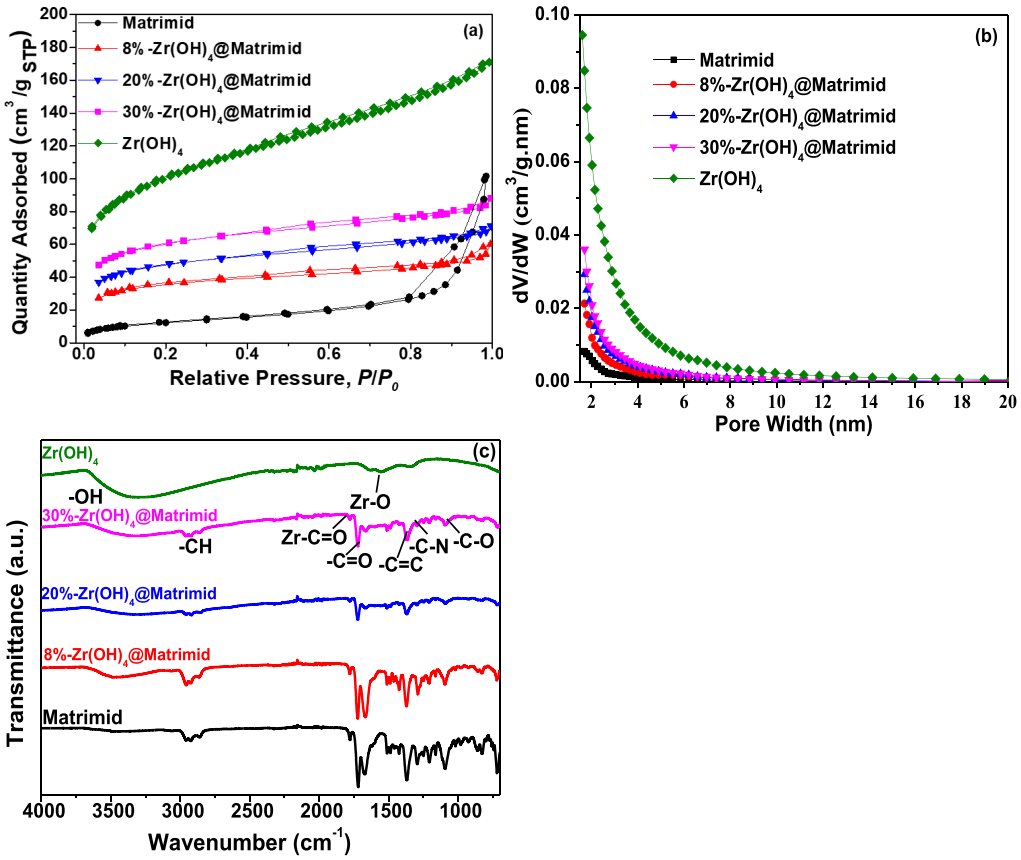

Figure 1. (a) N_2 physisorption isotherms, (b) PSD profiles, and (c) FTIR spectra of the *x*-$Zr(OH)_4$@Matrimid composites.

into a beaker with 1200 mL of DI water at 90 °C to ensure the termination of the polymerization reaction. The precipitant was stirred for 4 h to ensure the removal of residual salts. The mixture was filtered, and the resulting yellow polymer was dried in a vacuum oven for 2 h at 130 °C. The yellow powder was dissolved in 500 mL of chloroform and precipitated in methanol to remove low molecular weight oligomers. The reprecipitated polymer was filtered once more, dried in a vacuum oven at 130 °C, dissolved in 500 mL of THF, and precipitated in a 1:2 mixture of THF and acetone. The polymer was then recovered by vacuum filtration and vacuum-dried at 130 °C overnight. To develop the $Zr(OH)_4$@PIM-1 composites, PIM-1 powder (397 mg) was dissolved in 19.6 mL of $CHCl_3$ and stirred overnight. $Zr(OH)_4$ was added to the solution of PIM-1 in 8, 20, and 30 wt %. The composite solution was stirred to achieve a homogeneous mixture, followed by casting on a glass Petri dish under a nitrogen blanket to form a solid polymeric composite. Finally, the material was washed gently in methanol for 3 h and then dried in a vacuum oven at 50 °C.

2.2. Characterization of Bare Polymers and *x*-$Zr(OH)_4$@ Polymer Composites. To assess the textural properties of the composite materials, we measured N_2 physisorption isotherms at −196 °C on a static volumetric adsorption system (Micromeritics 3Flex). 100 mg sample of the composite was loaded into an N_2 physisorption tube and then degassed at 60 °C in a Micromeritics Smart VacPrep under vacuum for 6 h. The material surface area was determined from the isotherms using the linearized Brunauer−Emmett−Teller (BET) model in the relative pressure range of $0.05 < P/P^{sat} < 0.3$, whereas the density functional theory (DFT) model was used to determine pore volume and pore size distribution (PSD). To reveal the surface morphology of the samples, scanning electron microscopy (SEM) was performed on a Hitachi TM-1000 at an accelerating voltage of 15 kV. To determine thermal stability and amount of $Zr(OH)_4$ within the polymer composites, thermogravimetric analysis (TGA) was done on a Q500 thermal analyzer (TA Instruments) under N_2 flow at 20 mL/min, and a temperature ramp of 10 °C/min was maintained up to 800 °C. Structural elucidation was confirmed with the aid of a Fourier transform infrared spectrometer (Nicolet iS50) and an Avance Bruker 400 MHz nuclear magnetic resonance (NMR) spectrometer.

2.3. DMNP Hydrolysis Tests. We first studied the influence of two different buffers, namely, 2-amino-2-methyl-1,3-propanediol (AMPD) and *N*-ethylmorpholine (NEM), on the hydrolysis of DMNP, and the results displayed in Figure S1 of the Supporting Information illustrate the stability of the DMNP molecule upon exposure to AMPD and NEM. It is also clear from this figure that while NEM resulted in early conversion of DMNP to methyl-4-nitrophenyl phosphate (M4NP), AMPD had less influence on the stability of the DMNP molecule. Based on these findings, AMPD was chosen as a suitable buffer solution for subsequent hydrolysis tests. First, 0.2 M AMPD solution with a pH of 8.5 was prepared, and then 10 vol % D_2O was added to the buffer solution. Next, 1.5 equivalent mol of the composite material was added to 2 mL of buffer solution. In each hydrolysis test, the polymer composite was ensured to be immersed in the solution by sonicating it for 1 h. Finally, 8 μL of 24.64 μmol DMNP was added to the solution to initiate the reaction at room temperature. 0.2 mL aliquots were taken from the solution at specified time intervals and transferred into an NMR tube for analysis with a ^{31}P NMR spectrometer. Dimethyl phosphate (DMP) was formed as the product of the reaction and expected to appear at 2.8 ppm, while the characteristic peaks of DMNP and M4NP were taken to be at −4.1 and −3.8 ppm, respectively.

3. RESULTS AND DISCUSSION

3.1. *x*-$Zr(OH)_4$@Matrimid Composites' Properties. The N_2 physisorption isotherms are shown in Figure 1a. According to the IUPAC classification, all the isotherms for the *x*-$Zr(OH)_4$@Matrimid depicted a type IV isotherm.[31,32] The $Zr(OH)_4$ isotherms revealed a type I−IV isotherm, confirming

https://doi.org/10.1021/acsapm.3c00918
ACS Appl. Polym. Mater. XXXX, XXX, XXX−XXX

Scheme 1. Mechanism Showing the Bonding Interaction between Carbonyl Groups Present in the Matrimid Polymer and $Zr(OH)_4$

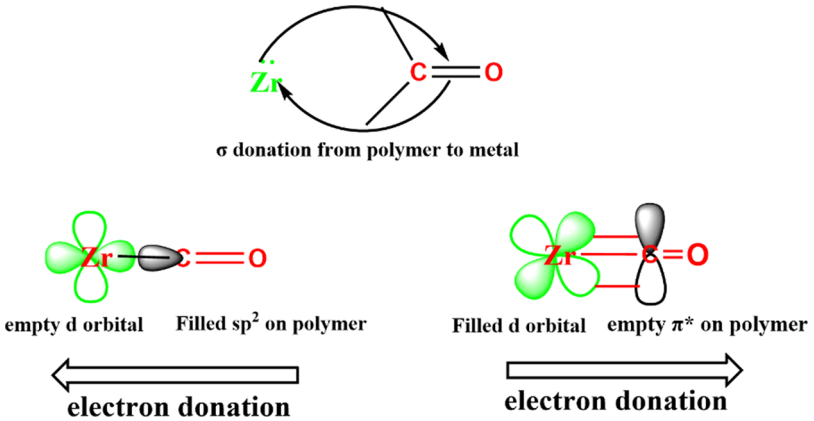

the predominant mesoporous−microporous nature of this material. The characteristic attributes of the type IV isotherms are their hysteresis loop, which is associated with capillary condensation taking place in the pores, and the limiting uptake over a range of high relative pressures. Upon incorporation of $Zr(OH)_4$ particles into the bare Matrimid, N_2 uptake increased over the *x*-$Zr(OH)_4$@Matrimid composites and 30%-Zr-$(OH)_4$@Matrimid exhibited the highest uptake, albeit lower than that of the bare $Zr(OH)_4$. It was also noted that the incorporation of $Zr(OH)_4$ changed the hysteresis loop of the bare Matrimid from H1 to H3. The PSD profiles in Figure 1b show the presence of both micro- and mesopores in the range of 1.5−20 nm for the *x*-$Zr(OH)_4$@Matrimid samples. The corresponding textural properties estimated from the isotherms are provided in Table S1. The BET surface area and micropore volume were in the order of 30%-$Zr(OH)_4$@Matrimid (203 m^2/g, 0.08 cm^3/g) > 20%-$Zr(OH)_4$@Matrimid (160 m^2/g, 0.06 cm^3/g) > 8%-$Zr(OH)_4$@Matrimid (119 m^2/g, 0.04 cm^3/g) > Matrimid (45 m^2/g, 0.02 cm^3/g). The increase in the BET surface area and micropore volume with $Zr(OH)_4$ content stems from the relatively high surface area (326 m^2/g) and micropore volume (0.11 cm^3/g) of the bare $Zr(OH)_4$ particles.

The FTIR analysis was used to elucidate the chemical structure of the composite materials. Figure 1c shows the FTIR spectra of the bare Matrimid, $Zr(OH)_4$, and their corresponding composites. The FTIR spectrum of the Matrimid polymer was identical with what was reported in the literature by displaying transmittance bands at 2860, 3030, and 3060 cm^{-1}, which corresponded to the stretching vibration bands of $-CH_3$ (alkane), =CH (alkene), and $=CH_2$ (aromatic alkene), respectively.[33] Moreover, intramolecular interaction between the carbonyl oxygen and hydrogen atoms on the aromatic rings was signified by a weak peak observed at 3400 cm^{-1}.[34] The $Zr(OH)_4$ spectrum revealed the dominant hydroxyl group, with its transmittance band at 3400 cm^{-1} present in the $Zr(OH)_4$ particles. From the spectra of the *x*-$Zr(OH)_4$@Matrimid composites, the appearance of a strong band at 3400 cm^{-1} could stem from the intermolecular hydrogen bond interactions between the carbonyl oxygen of Matrimid and the hydroxyl group in $Zr(OH)_4$. Moreover, the reduction in the intensity of carbonyl band at 1650−1700 cm^{-1} implied the interaction between the carbonyl group of Matrimid and Zr. The formation of a Zr−C═O bond at 1650 cm^{-1} supports the possible complexation of the $Zr(OH)_4$ with the Matrimid polymer via back-bonding, as illustrated in Scheme 1. Scheme 1 explains the possible bonding interaction between the vacant orbitals of the carbonyl group present in the Matrimid polymer and the filled d orbitals in the Zr atom. This interaction leads to a reduction in electron density on Zr through a mechanism called back-bonding, by which the carbonyl group donates a π bond (electron) into an empty orbital in the Zr while the Zr donates an electron into the low unoccupied π^* orbital of the carbonyl.[35,36] The direct evidence of this was seen from the reduced stretching vibration of carbonyl associated with *x*-$Zr(OH)_4$@Matrimid.[35] The $\pi-\pi^*$ transition created through this interaction creates an electron-rich environment which is sufficient to cause a nucleophilic attack on DMNP. The mechanism explained in Scheme 1 is also applicable to Ultem as they have the same active functional groups in their structures. Overall, comparison of the FTIR spectra of *x*-$Zr(OH)_4$@Matrimid provides evidence for the incremental addition of $Zr(OH)_4$ to the Matrimid polymer as the transmittance intensity at 3400 cm^{-1} (which is a characteristic transmittance band of the hydroxyl group stemming from $Zr(OH)_4$) increased with $Zr(OH)_4$ content.

The thermal stability of *x*-$Zr(OH)_4$@Matrimid composites and the bare Matrimid and $Zr(OH)_4$ particles was also assessed via TGA, as shown in Figure S2a. The bare polymer displayed a significant resistance up to 400 °C, which can be traced to the cross-linking of the imide (−N−C=O) functional group within the polymer, whereas $Zr(OH)_4$ showed zero resistance to heat up until 200 °C due to the predominant presence of hydroxyl groups. However, significant weight change was observed in the Matrimid polymer at 400 °C indicating the loss of adsorbed moisture and other carbonyl-containing moieties present within the polymer. Although the glass transition temperature of the bare Matrimid is 310 °C, it showed very high thermal resistance at elevated temperatures, consistent with the literature.[25,29] In contrast, a gradual drop in weight in the 100−400 °C range was observed in the TGA profiles of the $Zr(OH)_4$-loaded Matrimid samples, mainly due to the loss of hydroxyl groups, followed by a less sharper drop at higher temperatures, as opposed to the bare polymer, indicative of improved stability upon incorporating $Zr(OH)_4$, which was enhanced with $Zr(OH)_4$ content. The overall thermal resistance of the *x*-$Zr(OH)_4$@Matrimid composites was found to be in the order of 30%-$Zr(OH)_4$@Matrimid > 20%-$Zr(OH)_4$@Matrimid > 8%-$Zr(OH)_4$@Matrimid > Matrimid. From these profiles, the actual amounts of $Zr(OH)_4$

https://doi.org/10.1021/acsapm.3c00918
ACS Appl. Polym. Mater. XXXX, XXX, XXX−XXX

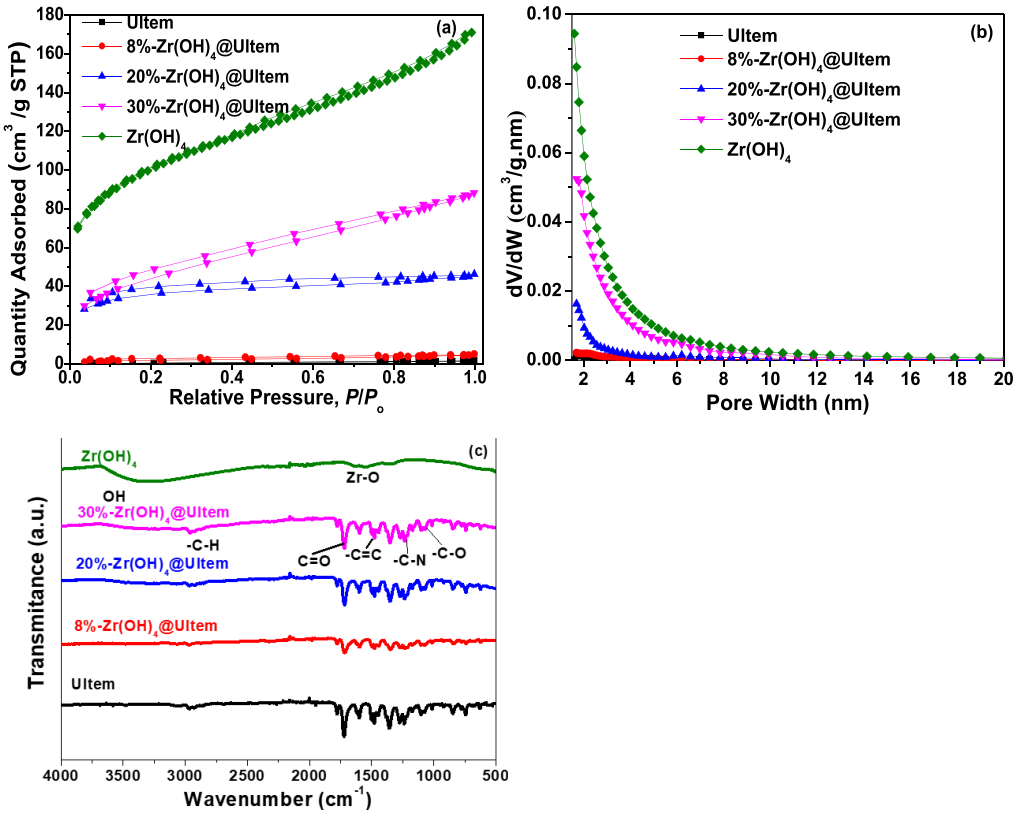

Figure 2. (a) N_2 physisorption isotherms, (b) PSD profiles, and (c) FTIR spectra of the *x*-$Zr(OH)_4$@Ultem composites.

loaded were found to be 100, 195, and 220 mg/g in 8, 20, and 30 wt % $Zr(OH)_4$-loaded samples, respectively, which were close to their nominal values used during their synthesis.

The cross-sectional SEM image in Figure S3a reveals that the $Zr(OH)_4$ particles in the composite fell in the size of 40−50 μm, whereas the uniform distribution of the particles can be observed from the aerial SEM image in Figure S3b. Such morphology ensures high accessibility of the active catalytic sites of both $Zr(OH)_4$ and Matrimid polymer to the DMNP molecules during hydrolysis reaction.

3.2. *x*-$Zr(OH)_4$@Ultem Composites' Properties. The N_2 physisorption isotherms and the PSD profiles of the *x*-$Zr(OH)_4$@Ultemare presented in Figure 2a,b. While the bare Ultem did not appreciably adsorb N_2 due to its nonporous nature deduced from its type II isotherms, the corresponding composites exhibited much higher N_2 uptake, especially with 20 and 30 wt % loadings, stemming from the highly porous nature of the $Zr(OH)_4$. The *x*-$Zr(OH)_4$@Ultem materials displayed type I−IV isotherms with essentially low microporosity. The surface area analysis of the bare Ultem polymer showed little to no porosity.[37] Incorporation with 8 wt % $Zr(OH)_4$ gave rise to a surface area of only 7 m^2/g, whereas 20 and 30 wt % loadings gave rise to surface areas of 121 and 160 m^2/g, respectively, with decent mesopore volumes (ca. 0.07 and 0.14 cm^3/g), as seen in Table S2. Moreover, the PSD profiles in Figure 2b confirmed the size of the mesopores in the range of 2.5−10 nm for these composites.

From Figure 2c, the bare Ultem displayed stretching vibration bands of aromatic −C−O and C−N at 1105 and 1300 cm^{-1}, respectively, along with a peak at 1780 cm^{-1} which was related to asymmetric and symmetric stretching of the accompanying carbonyl group. The *x*-$Zr(OH)_4$@Ultem FTIR spectra showed a new absorbance at 3350 cm^{-1} resulting from the hydroxyl group stemming from the $Zr(OH)_4$ added to the polymer matrix.[38] Moreover the suppression and partial shift of the C═O group in *x*-$Zr(OH)_4$@Ultem can be due to complexation of the C═O with Zr to form Zr−C═O. The back-bonding mechanism shown in Scheme 1 explained the bond interaction between $Zr(OH)_4$ and Ultem. The TGA profiles in Figure S2b confirmed the thermal stability of the *x*-$Zr(OH)_4$@Ultem materials up to 100 °C. The weight loss in the 100−200 °C range can be attributed to the removal of absorbed moisture content or ether moieties within the polymer structure.[39] The degradation of the remaining organic content did not occur until 520 °C. The imide cross-linking of Ultem made it thermally resistible to high heat exposure.[38,40] Upon the addition of $Zr(OH)_4$, the residual weight at 800 °C increased, as expected, but such an increase was not proportional to the amount of the $Zr(OH)_4$ added due to the thermal instability of the hydroxyl group of the $Zr(OH)_4$. The estimated amounts of $Zr(OH)_4$ added to the composite were 50, 105, and 205 mg/g for 8%-$Zr(OH)_4$@Ultem, 20%-$Zr(OH)_4$@Ultem, and 30%-$Zr(OH)_4$@Ultem, respectively. The cross-sectional and aerial SEM images in Figure S3c,d revealed the successful incorporation and homogeneous distribution of $Zr(OH)_4$ particles into the Ultem polymer. Further, the particle sizes were estimated to be in the range of 40−50 μm. Compared to the Matrimid composites (Figure S3a,b), the interstitial space between the $Zr(OH)_4$ particles was quite closer in the Ultem composites, which confirmed that the amount of $Zr(OH)_4$ in Ultem was higher than in Matrimid, as determined by TGA. Thus, more catalytic active sites are expected in Ultem than in Matrimid.

3.3. *x*-$Zr(OH)_4$@PIM-1 Composites' Properties. The physisorption isotherms of the bare PIM-1 shown in Figure 3a perfectly describe type IV isotherms. The first step occurred in

https://doi.org/10.1021/acsapm.3c00918
ACS Appl. Polym. Mater. XXXX, XXX, XXX−XXX

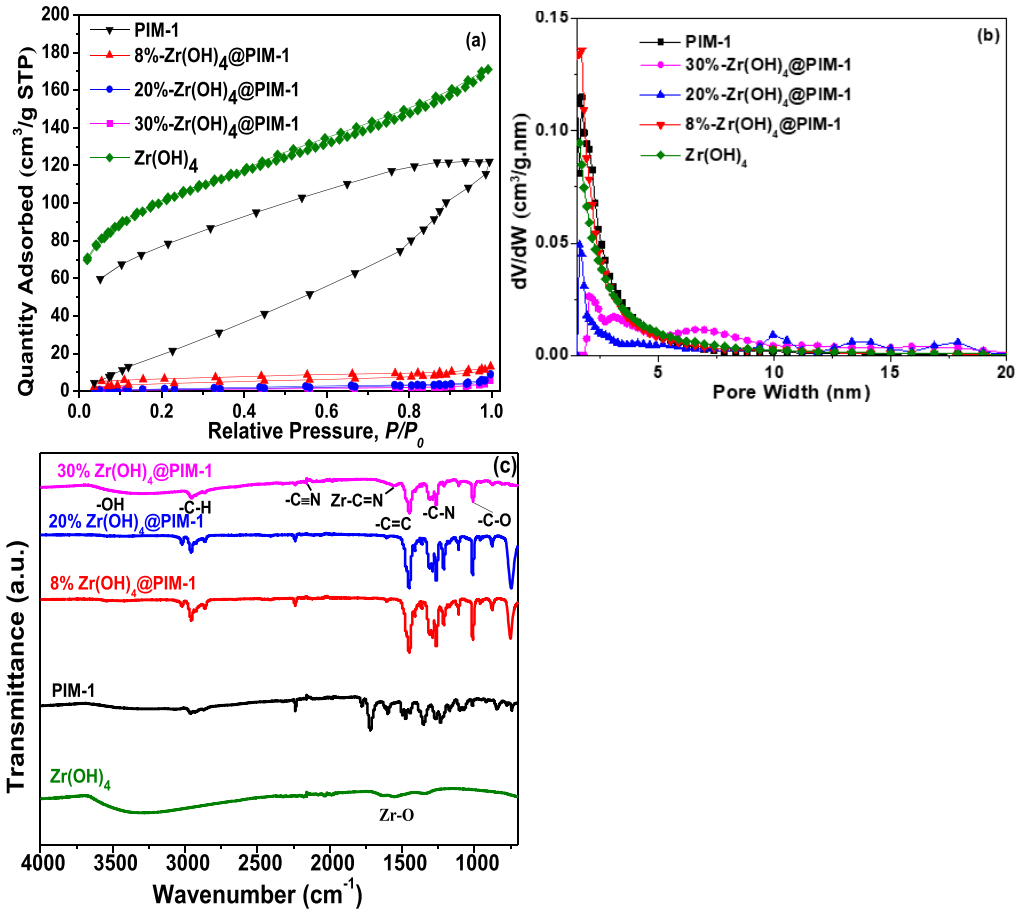

Figure 3. (a) N_2 physisorption isotherms, (b) PSD profiles, and (c) FTIR spectra of the *x*-$Zr(OH)_4$@PIM-1 composites.

the range of $P/P_0 \leq 0.75$, followed by the second (multilayer) step in the range of $0.8 \leq P/P_0 \leq 0.9$, while the last adsorption step occurred in $P/P_0 > 0.9$. The open-ended hysteresis observed stems from the presence of ultramicropores connected to larger mesopores, which caused temporary blockages, thereby slowing down the diffusion process, as is consistent with previously reported isotherms in the literature.[41] Alternatively, it is possible that the open pathway was caused by capillary evaporation that is affected by temperature and the size of the pores.[42]

Unlike the other two classes of the polymeric composites, incorporation of $Zr(OH)_4$ reduced the microporosity of the PIM-1 polymer, as can be observed from Figure 3b. This could be a result of the $Zr(OH)_4$ particles blocking the PIM-1 pores, especially at higher loadings, which drastically reduced the microporosity and flattening of the mono- and multilayer adsorption regions for 30%-$Zr(OH)_4$@PIM-1. From the data summarized in Table S3, the BET surface area decreased from 447 m^2/g to 117, 95, and 15 m^2/g and mesopore volume from 0.44 to 0.13, 0.09, and 0.06 cm^3/g for 8, 20, and 30 wt % $Zr(OH)_4$-loaded PIM-1 samples, respectively.

From the FTIR spectra in Figure 3c, the presence of a peak at 3400 cm^{-1} further confirmed the addition of $Zr(OH)_4$ to the PIM-1 polymer, as noted earlier.[43] Further, the incorporation of $Zr(OH)_4$ resulted in the reduction of the C≡N peak intensity at 2240 cm^{-1}, relevant to the bare polymer. The interaction between the Zr atom and the nitrile group was through the back-bonding mechanism which is depicted in Scheme 2.[35,44] The disappearance of the triple bond when this material undergoes tautomerism can be attributed to the reduction or absence of vibration stretching frequency at 2240 cm^{-1} and a possible reappearance of Zr−C═N at 1560 cm^{-1}.

Scheme 2. Mechanism Showing the Bonding Interaction between −C≡N Groups in PIM-1 and $Zr(OH)_4$ to Form Zr−C═N

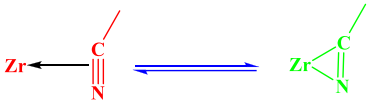

The TGA profiles of *x*-$Zr(OH)_4$@PIM-1 composites are presented in Figure S2c. The first stage of the weight loss between 100 and 200 °C was noticed in all four composite samples. However, initially, a rapid weight loss was observed for the 30%-$Zr(OH)_4$-loaded sample, which was attributed to the removal of more hydroxyl groups that were present in this sample. PIM-1 has a large pore volume; however, its cross-linking with chloroform after casting makes it more resistant to thermal degradation. Along with the other beneficial physiochemical properties of PIMs, their excellent thermal stability makes them attractive for catalytic applications.[16] For this polymer, the actual amount of $Zr(OH)_4$ added was found to correlate well with the nominal values. In Figure S3e,f, the cross-sectional and aerial SEM images of 30%-$Zr(OH)_4$@PIM-1 revealed that the particles of $Zr(OH)_4$ were evenly distributed throughout the matrix. It was also noted that the interstitial spaces between the $Zr(OH)_4$ particles were mostly

https://doi.org/10.1021/acsapm.3c00918
ACS Appl. Polym. Mater. XXXX, XXX, XXX−XXX

Scheme 3. Hydrolysis of DMNP over x-$Zr(OH)_4$@Polymer to Form DMP and M4NP in AMPD Buffer

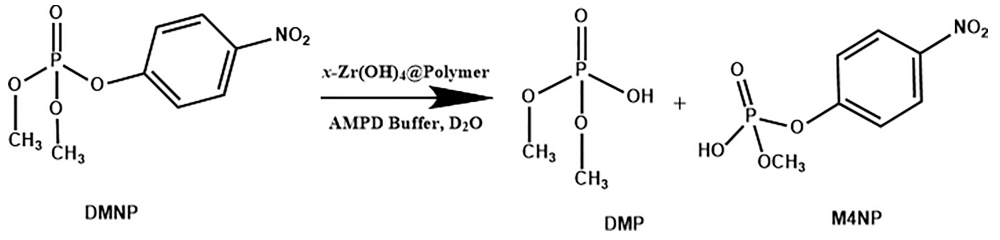

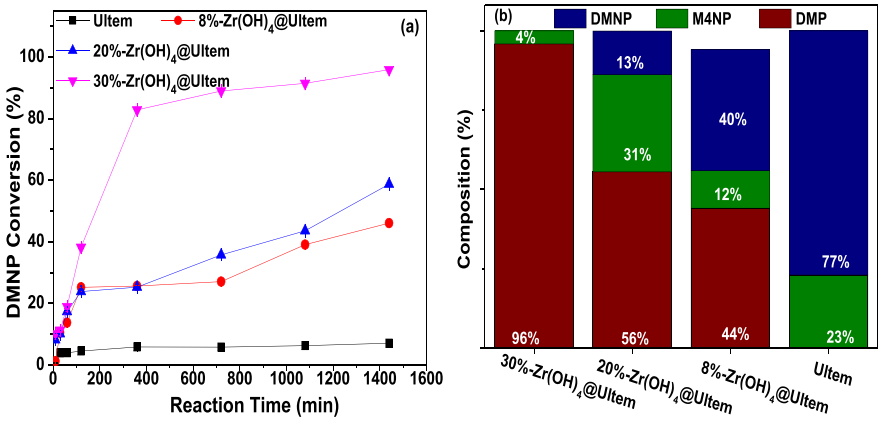

Figure 4. (a) Hydrolysis of DMNP over x-$Zr(OH)_4$@Ultem and (b) composition of reaction components after 24 h of DMNP hydrolysis.

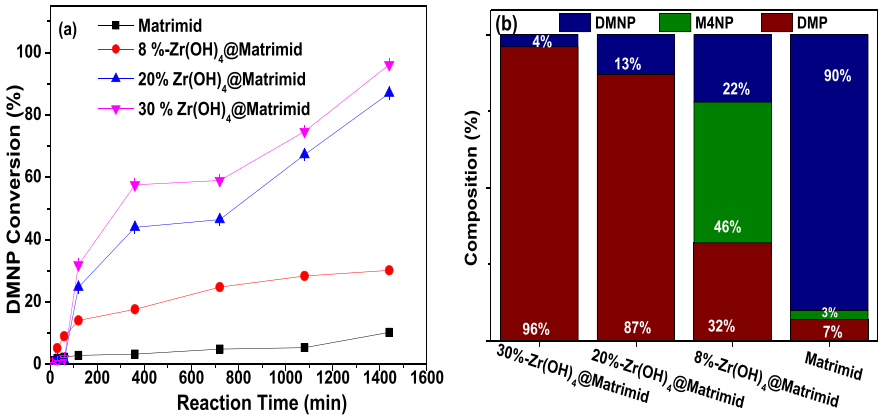

Figure 5. (a) Hydrolysis of DMNP over x-$Zr(OH)_4$@Matrimid and (b) composition of the reaction components after 24 h of hydrolysis of DMNP.

uniform and that the particles were more densely distributed in the PIM-1 than in the Matrimid and Ultem polymers, which further implied the less porous nature of the x-$Zr(OH)_4$@PIM-1 composites, as noted before.

3.4. DMNP Hydrolysis Tests. To evaluate the catalytic activity of the $Zr(OH)_4$-loaded polymer composites in detoxification of CWAs, DMNP hydrolysis tests were performed in an AMPD buffer solution at pH of 8.5. Scheme 3 depicts the reaction between DMNP and the composite materials. The typical interaction between DMNP and the catalyst is a nucleophilic substitution reaction, but the study by Jung et al.[16] proved that nucleophiles tend to give off M4NP, which is the second most toxic chemical in this reaction. Here, due to the nucleophilic nature of the x-$Zr(OH)_4$@polymer composites, M4NP was generated in the early stages of the reaction before it was later converted to DMP.

Prior to the hydrolysis of DMNP over polymeric composites, the bare $Zr(OH)_4$ was tested as a control material, and the corresponding result is presented in Figure S4. As evident from this figure, the bare $Zr(OH)_4$ particles achieved 100% DMNP conversion after a 6 h reaction time. It is worth noting here that the as-purchased $Zr(OH)_4$ particles were first activated at 300 °C prior to the hydrolysis test and also fabrication of polymeric composites. This was done mainly because activation of the particles leads to the consumption of surface hydroxyl groups, thereby rendering the Zr atoms more exposed for interaction with the phosphonyl moiety from the DMNP, as confirmed by density functional theory (DFT) computations.[45]

3.4.1. DMNP Hydrolysis over x-Zr(OH)$_4$@Ultem Composites. The DMNP hydrolysis results for the x-$Zr(OH)_4$@Ultem composites are shown in Figure 4. It is evident that the Ultem polymer itself was not reactive even after 24 h exposure to DMNP and could barely initiate any attack on the phosphonate group of the DMNP. However, as evident from Figure 4a, the conversion rate improved with the addition of

https://doi.org/10.1021/acsapm.3c00918
ACS Appl. Polym. Mater. XXXX, XXX, XXX−XXX

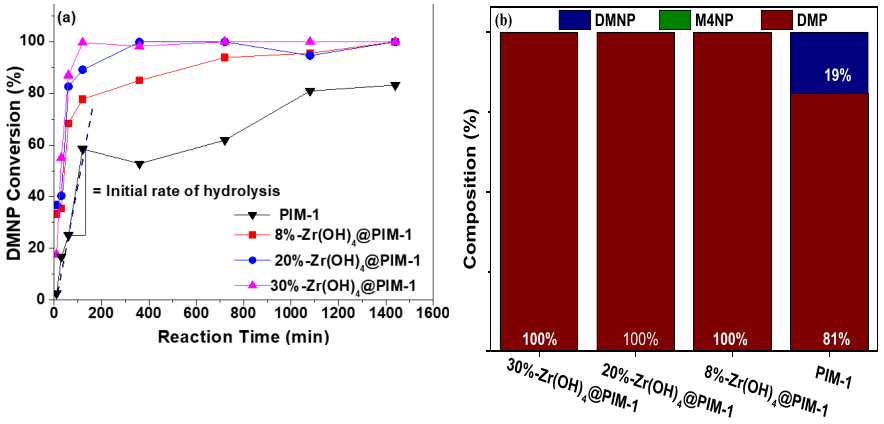

Figure 6. (a) Hydrolysis of DMNP over *x*-$Zr(OH)_4$@PIM-1. (b) Composition of the reaction components after 24 h hydrolysis of DMNP.

$Zr(OH)_4$ and 30%-$Zr(OH)_4$@Ultem exhibited much faster degradation rate (~20 times faster) than the bare polymer. This reactivity can be traced to the ability of the Zr atom to complexate with the carbonyl group (−C═O) in the Ultem structure, as explained by the FTIR analysis. This process helps to create an electron-rich environment (−Zr−C═O) in the presence of water (in the buffer solution) to launch a nucleophilic attack on the phosphorus atom within the phosphoryl moiety, leading to the destruction of DMNP. After 24 h exposure, 30%-$Zr(OH)_4$@Ultem, 20%-$Zr(OH)_4$@Ultem, and 8%-$Zr(OH)_4$@Ultem displayed 96, 59, and 46% hydrolysis, respectively. Figure S5a shows the representative NMR spectra that were used to quantify the conversion rate of DMNP and the composition of the hydrolysis solution at 2, 6, and 24 h, whereas the compositions of DMNP and hydrolysis products after 24 h of reaction are presented in Figure 4b. It again clarifies the promotional effect of the highest content of $Zr(OH)_4$ in the polymer composites. DMP is the harmless, most stable, and highly desired product in the hydrolysis reaction of DMNP. Incorporation of $Zr(OH)_4$ resulted in the highest percentage of DMP formed as well as the overall conversion of DMNP. The trend in this reaction also was in line with the porous properties of the materials in that the higher the porosity, the better the reactivity; i.e., more DMNP molecules get access to the active sites and subsequently converted.

3.4.2. DMNP Hydrolysis Tests over x-Zr(OH)$_4$@Matrimid Composites. Figure 5a shows the conversion of DMNP to DMP over 8, 20, and 30% $Zr(OH)_4$-loaded Matrimid composites. As is clear, the bare Matrimid exhibited low activity in DMNP hydrolysis after 24 h of exposure in the AMPD buffer. However, similar to the Ultem-based composites, the addition of $Zr(OH)_4$ promoted the DMNP hydrolysis over *x*-$Zr(OH)_4$@Matrimid composites. Figure S5b shows the NMR spectra of 30%-$Zr(OH)_4$@Matrimid, which was used for quantifying the % conversion from DMNP to DMP over a specified period of time. After 24 h of exposure, the amount of DMNP converted was found to be 33 and 87% over 8%-$Zr(OH)_4$@Matrimid and 20%-$Zr(OH)_4$@Matrimid, respectively, whereas 96% conversion was observed over 30%-$Zr(OH)_4$@Matrimid. The results obtained from the Matrimid-based composites showed a similar result to what was obtained from the Ultem-based composites. Considering the similarities in the chemical structure of Matrimid and Ultem, both being a polyimide, similar performances would be expected from these two classes of materials; however, the nucleophilicity of Ultem would prevail in the course of this reaction to favor the formation of M4NP due to the ether (−C−O−C−) groups that are present in its chemical structure. Figure 5b represents the unconverted DMNP and the hydrolysis products after 24 h of reaction over the Matrimid-based materials. Similar to the Ultem analogues, $Zr(OH)_4$ in the *x*-$Zr(OH)_4$@Matrimid composites significantly enhanced the DMNP destruction process; however, Matrimid-based materials performed lower in chemical reactivity than *x*-$Zr(OH)_4$@Ultem composites.

3.4.3. DMNP Hydrolysis Tests over x-Zr(OH)$_4$@PIM-1 Composites. PIM-1 is a class of porous hydrophobic polymers that have been recently evaluated for the hydrolysis of chemical nerve agents. The introduction of $Zr(OH)_4$ makes it more hydrophilic and, thus, is expected to enhance its catalytic activity in the hydrolysis reaction. The hydrolysis results over this set of materials are illustrated in Figure 6. As opposed to Ultem and Matrimid polymers, the bare PIM-1 demonstrated high reactivity in the DMNP hydrolysis through interactions with the electron-deficient phosphorus atoms in DMNP in the presence of water, as shown in Figure 6a. The bare polymer achieved approximately 81% hydrolysis after 24 h of exposure to DMNP, and a half-life of ~2 h was recorded for this material. While the addition of $Zr(OH)_4$ reduced the porosity of the *x*-$Zr(OH)_4$@PIM-1, it enhanced the catalytic activity of the composites. As shown in Figure 6a, not only was the DMNP conversion increased with $Zr(OH)_4$ loading (by achieving 100% over all composites after 24 h) but also the conversion rate was improved. For example, 99.66% conversion was achieved in 2 h over 30%-$Zr(OH)_4$@PIM-1, which was much faster than those achieved over its 30%-$Zr(OH)_4$@Ultem and 30%-$Zr(OH)_4$@Matrimid counterparts. Figure S5c shows the time-dependent reaction progress illustrated in the NMR spectra of 30%-$Zr(OH)_4$@PIM-1. The NMR results further indicated complete conversion of DMNP to DMP. As shown in Figure 6b, after 24 h of hydrolysis, the complete conversion of DMNP to the desired product (DMP) was observed in all three *x*-$Zr(OH)_4$@PIM-1 composites. Among all three polymers, based on the hydrolysis kinetics, selectivity, and the conversion, PIM-1 was determined to be the best material for the nucleophilic attack to the nerve agent.

3.4.4. Effect of Temperature on DMNP Hydrolysis. As the hydrolysis reaction is a great function of temperature, we aimed at further probing the temperature dependency of DMNP hydrolysis over 30%-$Zr(OH)_4$@PIM-1 by conducting the hydrolysis tests at 40 and 60 °C in addition to room

https://doi.org/10.1021/acsapm.3c00918
ACS Appl. Polym. Mater. XXXX, XXX, XXX−XXX

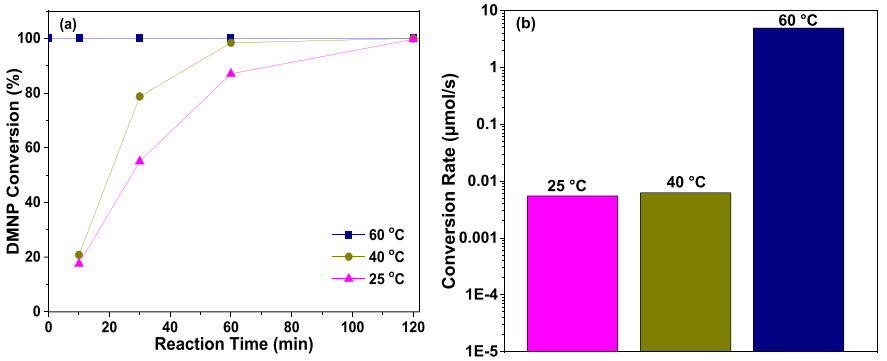

Figure 7. (a) Hydrolysis progress and (b) conversion rate of DMNP over 30%-Zr(OH)$_4$@PIM-1 at different temperatures.

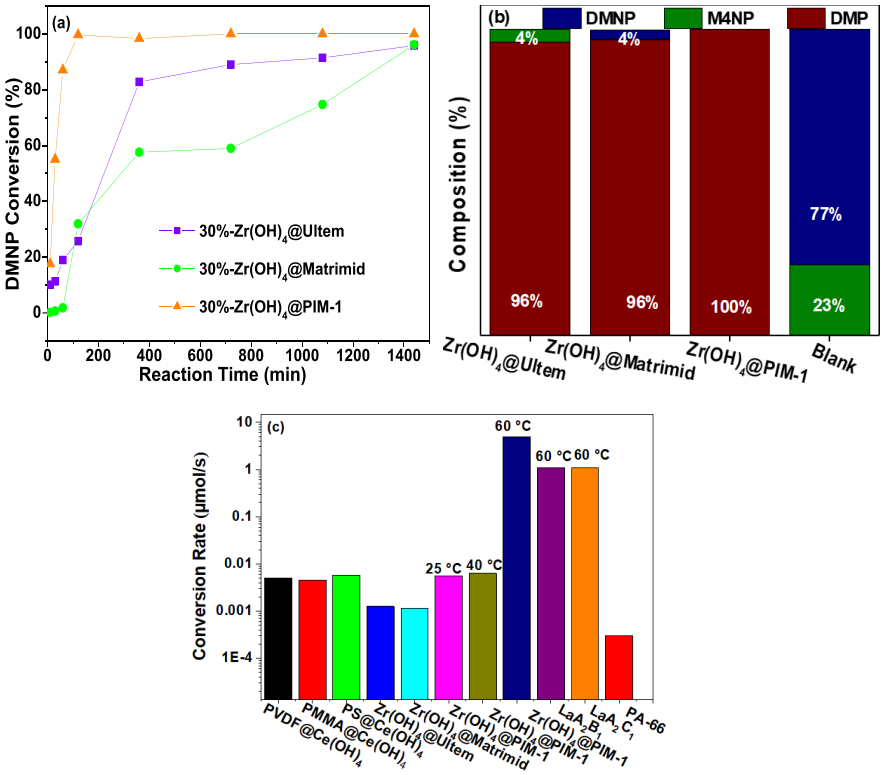

Figure 8. (a) DMNP conversion rate of 30%-Zr(OH)$_4$ incorporated PIM-1, Matrimid, and Ultem. (b) Composition of the reaction components after 24 h of hydrolysis using 30%-Zr(OH)$_4$ incorporated polymers. (c) Comparison of conversion rates obtained from this study and in the literature.

temperature. Given the endothermic nature of the reaction, the higher temperature is expected to enhance the hydrolysis rate.[46] Figure 7a compares the DMNP hydrolysis profiles as a function of time at three different temperatures, whereas Figure 7b depicts the conversion rates. As can be noted, the hydrolysis performance of the composite was substantially enhanced with temperature. The initial rate of hydrolysis was obtained from the slope corresponding to the first linear region of the curve provided in Figure 7a. In particular, a nearly instantaneous destruction was achieved at 60 °C with a conversion rate of 4.9 μmol/s, which was much faster than those at 25 and 40 °C (ca. 5.5 × 10^{-3} and 6.3 × 10^{-3} μmol/s, respectively). The superior performance of the 30%-Zr-(OH)$_4$@PIM-1 at higher temperatures is attributed to the increase in the thermal energy of the molecules participating in the reaction. These findings are in agreement with the literature.[47]

3.4.5. Overall Performance and Comparison with the Literature. Figure 8a depicts the comparison of the three polymers with their most effective loading of Zr(OH)$_4$ (i.e., 30 wt %). 30%-Zr(OH)$_4$@Matrimid exhibited the slowest conversion rate of 1.2 × 10^{-3} μmol/s, which clearly reflected the reactivity of Matrimid. The 30%-Zr(OH)$_4$@Ultem exhibited a similar reactivity as Matrimid, but the aromatic rings' resonance effect improved the material's reactivity. The conversion of 30%-Zr(OH)$_4$@Ultem was slightly faster compared to that of Matrimid analogues with a conversion rate of 1.3 × 10^{-3} μmol/s. Nearly 100% DMNP conversion by 30%-Zr(OH)$_4$@PIM-1 was recorded in 2 h of exposure with the highest hydrolysis rate of 5.5 × 10^{-3} μmol/s. The superior performance of PIM-1-based composite over those of Ultem and Matrimid analogues can be attributed to the resonance features around the nitrile functional groups present within the molecular structure of PIM-1. Such functional groups are

https://doi.org/10.1021/acsapm.3c00918
ACS Appl. Polym. Mater. XXXX, XXX, XXX−XXX

extremely reactive due to their sp-hybridized orbital. Furthermore, PIM-1 doped with a transition metal helps to activate charge transfer and $\pi-\pi^*$ interactions between the polymer and $Zr(OH)_4$. It is well-known that sp-hybridized orbitals (triple bond) are more reactive compared to sp^2-hybridized orbitals (double bond). Ultem and Matrimid polymers contain sp^2-hybridized orbitals, indicating their lower reactivity compared to the PIM-1. Figure 8b demonstrates the effect of inherent physiochemical properties of the polymer matrix on the hydrolysis performance of the composite materials. In terms of % conversion toward desired products, the sequence of the materials was organized as follows: PIM-1 > Ultem > Matrimid.

To better understand the standings of our best performing composite in each set (i.e., 30%-$Zr(OH)_4$@Matrimid, 30%-$Zr(OH)_4$@Ultem, and 30%-$Zr(OH)_4$@PIM-1), a comparison was made to the published results for polymer−metal hydroxide composites (Figure 8c). As evident from this figure, PA-66, which is a bare polymer had the slowest conversion rate of 3.0×10^{-4} μmol/s, followed by $Ce(OH)_4$-loaded polymers, namely, PVDF@$Ce(OH)_4$, PMMA@$Ce(OH)_4$, and PS@$Ce(OH)_4$ with conversion rates of 5.1×10^{-3}, 4.6×10^{-3}, and 5.8×10^{-3} μmol/s, respectively.[48] Notably, a group of catechol-activated porous organic polymers (POPs), namely, LaA_2B_1 and LaA_2C_1, were tested for the hydrolysis of DMNP at pH 11 under 60 °C and the highest conversion rate of 1.1 μmol/s.[49] At 60 °C, our 30%-$Zr(OH)_4$@PIM-1 surpassed these POP-based materials by exhibiting a conversion rate of 4.9 μmol/s with instantaneous hydrolysis (i.e., 100% conversion within 5 s, as noted earlier). Moreover, it should be pointed out here that even at room temperature the 30%-$Zr(OH)_4$@PIM-1 outperforms other polymer-based composites.

4. CONCLUSIONS

In this work, we investigated three different polymers and their $Zr(OH)_4$-incorporated composites for the detoxification of a nerve agent simulant (DMNP). The incorporation of $Zr(OH)_4$ significantly reduced the surface area and pore volume in the PIM-1 composites. On the contrary, the surface area and pore volume of both Ultem and Matrimid remarkably improved with the introduction of $Zr(OH)_4$ within their composites. Our results revealed that incorporation of $Zr(OH)_4$ into polymers significantly promoted the DMNP hydrolysis performance of the materials. For all three polymer sets, 30 wt % $Zr(OH)_4$ was found to be the most efficient loading. Results also showed that the PIM-1-based composites performed better than their Ultem and Matrimid analogues, with 30%-$Zr(OH)_4$@PIM-1 being the most efficient composite, exhibiting a nearly 100% conversion under 2 h. These results demonstrate the efficacy of $Zr(OH)_4$@PIM-1 in the destruction of CWA simulants. Further improvement of the PIM-1 composites to achieve faster hydrolysis rates will enable formulation of these materials into mask filters for use by the military or first responders.

■ ASSOCIATED CONTENT

Supporting Information

The Supporting Information is available free of charge at https://pubs.acs.org/doi/10.1021/acsapm.3c00918.

Effect of buffers, TGA profiles, SEM images, ^{31}P NMR spectra, and textural properties of the composites (PDF)

■ AUTHOR INFORMATION

Corresponding Authors

Ali A. Rownaghi − *Department of Chemistry, Cleveland State University, Cleveland, Ohio 44115, United States;* orcid.org/0000-0001-5228-5624; Email: a.rownaghi@csuohio.edu

Fateme Rezaei − *Linda and Bipin Doshi Department of Chemical and Biochemical Engineering, Missouri University of Science and Technology, Rolla, Missouri 65409-1230, United States;* orcid.org/0000-0002-4214-4235; Email: rezaeif@mst.edu

Authors

Peter O. Aina − *Linda and Bipin Doshi Department of Chemical and Biochemical Engineering, Missouri University of Science and Technology, Rolla, Missouri 65409-1230, United States*

Sukanta K. Mondal − *Linda and Bipin Doshi Department of Chemical and Biochemical Engineering, Missouri University of Science and Technology, Rolla, Missouri 65409-1230, United States;* orcid.org/0000-0002-1880-1127

Joshua Costain − *Linda and Bipin Doshi Department of Chemical and Biochemical Engineering, Missouri University of Science and Technology, Rolla, Missouri 65409-1230, United States*

Complete contact information is available at: https://pubs.acs.org/10.1021/acsapm.3c00918

Notes

The authors declare no competing financial interest.

■ ACKNOWLEDGMENTS

The authors thank the US Department of Defense (DAC 20-0280) for funding this research project. The involvement of A.A.R. in this work was sponsored by the National Science Foundation (NSF CBET-2019350).

■ REFERENCES

(1) Liu, Y.; Howarth, A. J.; Vermeulen, N. A.; Moon, S.-Y.; Hupp, J. T.; Farha, O. K. Catalytic Degradation of Chemical Warfare Agents and Their Simulants by Metal-Organic Frameworks. *Coord. Chem. Rev.* **2017**, *346*, 101−111.

(2) Vucinic, S.; Antonijevic, B.; Tsatsakis, A. M.; Vassilopoulou, L.; Docea, A. O.; Nosyrev, A. E.; Izotov, B. N.; Thiermann, H.; Drakoulis, N.; Brkic, D. Environmental Exposure to Organophosphorus Nerve Agents. *Environ. Toxicol Pharmacol* **2017**, *56*, 163−171.

(3) Andreasen, J. H. Still Defining "Discharge of a Pollutant" after Thirty Years. *Natural Resources & Environment* **2010**, *24* (4), 52−54.

(4) Hallikainen, J.; Lund, V. Chemical Warfare Agent Terrorist Attacks in Latin America and the Caribbean Region (CWA-LAC). *Prehosp Disaster Med.* **2019**, *34* (s1), s13−s13.

(5) Baca, S. C.; Singler, C.; Zacharia, S.; Seo, J.-H.; Morova, T.; Hach, F.; Ding, Y.; Schwarz, T.; Huang, C.-C. F.; Anderson, J.; et al. Genetic Determinants of Chromatin Reveal Prostate Cancer Risk Mediated by Context-Dependent Gene Regulation. *Nat. Genet.* **2022**, *54* (9), 1364−1375.

(6) Dhummakupt, E. S.; Mach, P. M.; Carmany, D.; Demond, P. S.; Moran, T. S.; Connell, T.; Wylie, H. S.; Manicke, N. E.; Nilles, J. M.; Glaros, T. Direct Analysis of Aerosolized Chemical Warfare Simulants Captured on a Modified Glass-Based Substrate by "Paper-Spray" Ionization. *Anal. Chem.* **2017**, *89* (20), 10866−10872.

(7) Talmage, S. S.; Watson, A. P.; Hauschild, V.; Munro, N. B.; King, J. Chemical Warfare Agent Degradation and Decontamination. *Curr. Org. Chem.* **2007**, *11* (3), 285−298.

(8) Kim, K.; Tsay, O. G.; Atwood, D. A.; Churchill, D. G. Destruction and Detection of Chemical Warfare Agents. *Chem. Rev.* **2011**, *111* (9), 5345−5403.
(9) Eubanks, L. M.; Dickerson, T. J.; Janda, K. D. Technological Advancements for the Detection of and Protection against Biological and Chemical Warfare Agents. *Chem. Soc. Rev.* **2007**, *36* (3), 458−470.
(10) Yang, Y. C.; Baker, J. A.; Ward, J. R. Decontamination of Chemical Warfare Agents. *Chem. Rev.* **1992**, *92* (8), 1729−1743.
(11) Silva, V. B.; Campos, R. B.; Pavez, P.; Medeiros, M.; Orth, E. S. Nucleophilic Neutralization of Organophosphates: Lack of Selectivity or Plenty of Versatility? *Chem. Rec.* **2021**, *21* (10), 2638−2665.
(12) He, Y.; Itta, A. K.; Alwakwak, A.; Huang, M.; Rezaei, F.; Rownaghi, A. A. Aminosilane-Grafted SiO_2-ZrO_2 Polymer Hollow Fibers as Bifunctional Microfluidic Reactor for Tandem Reaction of Glucose and Fructose to 5-Hydroxymethylfurfural. *ACS Sustain Chem. Eng.* **2018**, *6* (12), 17211−17219.
(13) Giannakoudakis, D. A.; Pearsall, F.; Florent, M.; Lombardi, J.; O'Brien, S.; Bandosz, T. J. Barium Titanate Perovskite Nanoparticles as a Photoreactive Medium for Chemical Warfare Agent Detoxification. *J. Colloid Interface Sci.* **2018**, *531*, 233−244.
(14) Giles, S. L.; Kastl, A. M.; Purdy, A. P.; Leff, A. C.; Ratchford, D. C.; Maza, W. A.; Baturina, O. A. Surface-and Structural-Dependent Reactivity of Titanium Oxide Nanostructures with 2-Chloroethyl Ethyl Sulfide under Ambient Conditions. *ACS Appl. Mater. Interfaces* **2022**, *14* (7), 9655−9666.
(15) He, Y.; Rezaei, F.; Kapila, S.; Rownaghi, A. A. Engineering Porous Polymer Hollow Fiber Microfluidic Reactors for Sustainable C-H Functionalization. *ACS Appl. Mater. Interfaces* **2017**, *9* (19), 16288−16295.
(16) Jung, D.; Das, P.; Atilgan, A.; Li, P.; Hupp, J. T.; Islamoglu, T.; Kalow, J. A.; Farha, O. K. Reactive Porous Polymers for Detoxification of a Chemical Warfare Agent Simulant. *Chem. Mater.* **2020**, *32* (21), 9299−9306.
(17) Bromberg, L.; Schreuder-Gibson, H.; Creasy, W. R.; McGarvey, D. J.; Fry, R. A.; Hatton, T. A. Degradation of Chemical Warfare Agents by Reactive Polymers. *Ind. Eng. Chem. Res.* **2009**, *48* (3), 1650−1659.
(18) Grissom, T. G.; Plonka, A. M.; Sharp, C. H.; Ebrahim, A. M.; Tian, Y.; Collins-Wildman, D. L.; Kaledin, A. L.; Siegal, H. J.; Troya, D.; Hill, C. L.; et al. Metal-Organic Framework-and Polyoxometalate-Based Sorbents for the Uptake and Destruction of Chemical Warfare Agents. *ACS Appl. Mater. Interfaces* **2020**, *12* (13), 14641−14661.
(19) Bandosz, T. J.; Laskoski, M.; Mahle, J.; Mogilevsky, G.; Peterson, G. W.; Rossin, J. A.; Wagner, G. W. Reactions of VX, GD, and HD with $Zr(OH)_4$: Near Instantaneous Decontamination of VX. *J. Phys. Chem. C* **2012**, *116* (21), 11606−11614.
(20) Kirlikovali, K. O.; Chen, Z.; Islamoglu, T.; Hupp, J. T.; Farha, O. K. Zirconium-Based Metal-Organic Frameworks for the Catalytic Hydrolysis of Organophosphorus Nerve Agents. *ACS Appl. Mater. Interfaces* **2020**, *12* (13), 14702−14720.
(21) Islamoglu, T.; Atilgan, A.; Moon, S.-Y.; Peterson, G. W.; DeCoste, J. B.; Hall, M.; Hupp, J. T.; Farha, O. K. Cerium (IV) vs Zirconium (IV) Based Metal-Organic Frameworks for Detoxification of a Nerve Agent. *Chem. Mater.* **2017**, *29* (7), 2672−2675.
(22) He, Y.; Jawad, A.; Li, X.; Atanga, M.; Rezaei, F.; Rownaghi, A. A. Direct Aldol and Nitroaldol Condensation in an Aminosilane-Grafted Si/Zr/Ti Composite Hollow Fiber as a Heterogeneous Catalyst and Continuous-Flow Reactor. *J. Catal.* **2016**, *341*, 149−159.
(23) Rownaghi, A. A.; Kant, A.; Li, X.; Thakkar, H.; Hajari, A.; He, Y.; Brennan, P. J.; Hosseini, H.; Koros, W. J.; Rezaei, F. Aminosilane-Grafted Zirconia-Titiania-Silica Nanoparticles/Torlon Hollow Fiber Composites for CO_2 Capture. *ChemSusChem* **2016**, *9* (10), 1166−1177.
(24) He, Y.; Cheshomi, N.; Lawson, S. M.; Itta, A. K.; Rezaei, F.; Kapila, S.; Rownaghi, A. A. PDMS/PAI-HF Composite Membrane Containing Immobilized Palladium Nanoparticles for 4-Nitrophenol Reduction. *Chem. Eng. J.* **2021**, *410*, 128326.
(25) Rownaghi, A. A.; Rezaei, F.; Labreche, Y.; Brennan, P. J.; Johnson, J. R.; Li, S.; Koros, W. J. In situ Formation of a Monodispersed Spherical Mesoporous Nanosilica-Torlon Hollow-Fiber Composite for Carbon Dioxide Capture. *ChemSusChem* **2015**, *8* (20), 3439−3450.
(26) Zaske, O. C.; Goodman, S. H. Handbook of Thermoset Plastics. *William Andrew Publishing, Noyes Publications, Westwood, NJ.* **1998**, 97.
(27) Koros, W. J.; Fleming, G. K. Membrane-based gas separation. *J. Membrane science* **1993**, *83* (1), 1−80.
(28) Yang, Y.; Dang, Z.; Li, Q.; He, J. Self-healing of Electrical Damage in Polymers. *Advanced Science* **2020**, *7* (21), 2002131.
(29) Dai, Y.; Johnson, J.R.; Karvan, O.; Sholl, D. S.; Koros, W.J. Ultem®/ZIF-8 mixed matrix hollow fiber membranes for CO_2/N2 separations. *J. Membrane science* **2012**, *401* (1), 76−82.
(30) Mason, C. R.; Maynard-Atem, L.; Al-Harbi, N. M.; Budd, P. M.; Bernardo, P.; Bazzarelli, F.; Clarizia, G.; Jansen, J. C. Polymer of Intrinsic Microporosity Incorporating Thioamide Functionality: Preparation and Gas Transport Properties. *Macromolecules* **2011**, *44* (16), 6471−6479.
(31) Okada, K.; Nandi, M.; Maruyama, J.; Oka, T.; Tsujimoto, T.; Kondoh, K.; Uyama, H. Fabrication of Mesoporous Polymer Monolith: A Template-Free Approach. *Chem. Commun.* **2011**, *47* (26), 7422−7424.
(32) Thommes, M.; Kaneko, K.; Neimark, V. A.; Olivier, J. P.; Rodriguez-Reinoso, F.; Rouquerol, J.; Sing, K. S. W. Physisorption of gases, with special reference to the evaluation of surface area and pore size distribution. *Pure Appl. Chem.* **2015**, *87* (9−10), 1051−1069.
(33) Wang, Y.; Goh, S. H.; Chung, T.-S. Miscibility Study of Torlon® Polyamide-Imide with Matrimid® 5218 Polyimide and Polybenzimidazole. *Polymer (Guildf)* **2007**, *48* (10), 2901−2909.
(34) Liu, J.; Yang, T.; Wang, D.-W.; Lu, G. Q.; Zhao, D.; Qiao, S. Z. A Facile Soft-Template Synthesis of Mesoporous Polymeric and Carbonaceous Nanospheres. *Nat. Commun.* **2013**, *4* (1), 2798.
(35) Clayden, J.; Greeves, N.; Warren, S. *Organic Chemistry*; Oxford University Press: 2012.
(36) Crabtree, R. H. *The Organometallic Chemistry of the Transition Metals*; John Wiley & Sons: 2009.
(37) Saimani, S.; Kumar, A. Semi-IPN Asymmetric Membranes Based on Polyether Imide (ULTEM) and Polyethylene Glycol Diacrylate for Gaseous Separation. *J. Appl. Polym. Sci.* **2008**, *110* (6), 3606−3615.
(38) Yilmaz, M.; Yilmaz, N. F.; Kalkan, M. F. Rheology, Crystallinity, and Mechanical Investigation of Interlayer Adhesion Strength by Thermal Annealing of Polyetherimide (PEI/ULTEM 1010) Parts Produced by 3D Printing. *J. Mater. Eng. Perform* **2022**, *31*, 1−10.
(39) Chuang, K. C.; Grady, J. E.; Draper, R. D.; Shin, E.-S. E.; Patterson, C.; Santelle, T. D. Additive Manufacturing and Characterization of Ultem Polymers and Composites. *Additive Manufacturing*; CRC Press: 2015.
(40) Xu, Z.; Gehui, L.; Cao, K.; Guo, D.; Serrano, J.; Esker, A.; Liu, G. Solvent-Resistant Self-Crosslinked Poly (Ether Imide). *Macromolecules* **2021**, *54* (7), 3405−3412.
(41) Liu, Y.; Zhang, J.; Tan, X. High Performance of PIM-1/ZIF-8 Composite Membranes for O_2/N_2 Separation. *ACS Omega* **2019**, *4* (15), 16572−16577.
(42) Morishige, K.; Ishino, M. Lower Closure Point of Adsorption Hysteresis in Ordered Mesoporous Silicas. *Langmuir* **2007**, *23* (22), 11021−11026.
(43) Tamaddondar, M.; Foster, A. B.; Carta, M.; Gorgojo, P.; McKeown, N. B.; Budd, P. M. Mitigation of Physical Aging with Mixed Matrix Membranes Based on Cross-Linked PIM-1 Fillers and PIM-1. *ACS Appl. Mater. Interfaces* **2020**, *12* (41), 46756−46766.
(44) Storhoff, B. N.; Lewis, H. C., Jr. Organonitrile Complexes of Transition Metals. *Coord. Chem. Rev.* **1977**, *23* (1), 1−29.
(45) Schweigert, I. V.; Gunlycke, D. Hydrolysis of Dimethyl Methylphosphonate by the Cyclic Tetramer of Zirconium Hydroxide. *J. Phys. Chem. A* **2017**, *121* (40), 7690−7696.

https://doi.org/10.1021/acsapm.3c00918
ACS Appl. Polym. Mater. XXXX, XXX, XXX−XXX

(46) Chen, H.; Liao, P.; Mendonca, M. L.; Snurr, R. Q. Insights into Catalytic Hydrolysis of Organophosphate Warfare Agents by Metal-Organic Framework NU-1000. *J. Phys. Chem. C* **2018**, *122* (23), 12362−12368.
(47) Balow, R. B.; McEntee, M.; Schweigert, I. V.; Jeon, S.; Peterson, G. W.; Pehrsson, P. Battling Chemical Weapons with Zirconium Hydroxide Nanoparticle Sorbent: Impact of Environmental Contaminants on Sarin Sequestration and Decomposition. *Langmuir* **2021**, *37* (23), 6923−6934.
(48) Dwyer, D. B.; Liu, J.; Gomez, J. C.; Tovar, T. M.; Davoodabadi, A.; Bernier, W. E.; DeCoste, J. B.; Jones, W. E. J. Metal Hydroxide/Polymer Textiles for Decontamination of Toxic Organophosphates: An Extensive Study of Wettability, Catalytic Activity, and the Effects of Aggregation. *ACS Appl. Mater. Interfaces* **2019**, *11* (34), 31378−31385.
(49) Totten, R. K.; Weston, M. H.; Park, J. K.; Farha, O. K.; Hupp, J. T.; Nguyen, S. T. Catalytic Solvolytic and Hydrolytic Degradation of Toxic Methyl Paraoxon with La(Catecholate)-Functionalized Porous Organic Polymers. *ACS Catal.* **2013**, *3* (7), 1454−1459.

https://doi.org/10.1021/acsapm.3c00918
ACS Appl. Polym. Mater. XXXX, XXX, XXX−XXX